# The Crystal Structure of the Orotate Phosphoribosyltransferase Complexed with Orotate and α-D-5-Phosphoribosyl-1-pyrophosphate[†,‡]

Giovanna Scapin,[§] Derya H. Ozturk,[∥] Charles Grubmeyer,[∥] and James C. Sacchettini*[,§]

*Department of Biochemistry, Albert Einstein College of Medicine, 1300 Morris Park Avenue, Bronx, New York 10461, and Department of Biochemistry and Fels Institute for Cancer Research, Temple University Medical School, 3420 North Broad Street, Philadelphia, Pennsylvania 19140*

*Received March 20, 1995; Revised Manuscript Received June 16, 1995*[⊗]

ABSTRACT: The three-dimensional structure of *Salmonella typhimurium* orotate phosphoribosyltransferase (OPRTase) in complex with the ribose 5-phosphate donor α-D-5−phosphoribosyl-1-pyrophosphate (PRPP) and the nitrogenous base orotic acid has been solved and refined with X-ray diffraction data extending to 2.3 Å resolution to a crystallographic *R*-factor of 18.7%. The complex was generated by carrying out catalysis in the crystal. Comparison of this structure with the previously reported structure of the orotidine 5′-monophosphate (OMP) complex [Scapin, G., Grubmeyer, C., and Sacchettini, J. C. (1994) *Biochemistry 33*, 1287−1294] revealed that the enzyme backbone undergoes only small movements. The most significant differences occur near the active site, at Ala71−Gly74, with the largest difference involving the side chains of Lys73, Val127−Ala133, the 5′-phosphate binding loop, and a long, solvent-exposed loop at the dimer interface. The position of the ribose moiety is, on the other hand, very different in the OMP and PRPP•orotate complexes, with its anomeric carbon moving approximately 7 Å across the binding cavity. In the PRPP•orotate complex the highly conserved acidic side chain of Asp124 interacts with the ribose of PRPP, whereas there are no interactions of this aspartate with the substrate in the OMP complex.

Orotate phosphoribosyltransferase (OPRTase,[1] EC 2.4.2.10) catalyzes the formation of the nucleotide orotidine monophosphate (OMP) from the ribose donor α-D-5-phosphoribosyl-1-pyrophosphate (PRPP) and the nitrogenous base orotic acid (Figure 1). At least 13 homologous enzymes that carry out this reaction have been identified in bacteria, fungi, insects, and mammals. Bacterial OPRTases all have a molecular mass of about 24 000 Da and appear to function as dimers. However, in mammals, slime mold, and insects, this activity is associated with a single domain of a bifunctional protein, containing both OPRTase and orotidylate decarboxylase, referred to as UMP synthase (McClard et al., 1980). In all cases studied thus far, OPRTase exhibits a requirement for $Mg^{2+}$ (Musick, 1981).

OPRTase is a member of a group of PRTases involved in the *de novo* and salvage pathways of nucleotide synthesis, as well as in the biosynthesis of histidine and tryptophan (Musick, 1981). The importance of these enzymes in nucleotide metabolism is evident from the clinical consequences of PRTase malfunction. For example, a rare inborn defect of the OPRTase domain of UMP synthase causes hereditary orotic aciduria, which may be linked in some cases to mental retardation (Suttle et al., 1989). Although the genes coding for the PRTases have been sequenced from many sources, there is very little sequence similarity among PRTases acting on different substrates. Only a short stretch of about 11−12 amino acids, containing two adjacent carboxylate residues, is conserved in most PRTases (Hershey & Taylor, 1986). The two carboxylate residues are typically preceded by four to five hydrophobic residues and followed by small and polar (Ala, Gly, Ser, Thr) residues. A similar sequence has also been found in the human PRPP synthetase (Hove-Jensen et al., 1986), and on the basis of its presence on both PRPP synthetase and the PRTases, it has been proposed to represent a PRPP binding motif.

The fundamental mechanistic hurdle faced by PRTases, like that of other glycosyl transferases, is the activation of the anomeric carbon toward transfer. In the case of OPRTase, the reaction proceeds with inversion of stereochemistry at the anomeric carbon (Chelsky & Parson, 1975), thus ruling out either a covalent enzyme intermediate or a double displacement mechanism. A loosely associative oxocarbonium-like transition state for phosphoribosyl transfer has been proposed (Bhatia et al., 1990), on the basis of kinetic and exchange studies, past data suggesting a $S_N1$-like mechanism (Goitein et al., 1978), and analogy to the nucleosidase transition state (Mentch et al., 1987). This mechanism suggests that a positive charge develops during formation of an oxocarbonium-like transition state. The two conserved acidic residues of the PRPP binding motif could be involved in stabilizing this charge. Structural studies on complexes of OPRTase with different substrates and/or inhibitors can help resolve mechanistic questions by identifying the position of substrates and products within the

[†] This work was supported by NIH Grants GM48623 and GM45859. Facilities in the Fels Institute are supported by NIH Grant 5-P30-Ca12227

[‡] Coordinates for the three-dimensional structure of the orotate phosphoribosyltransferase complexed with orotate and α-D-5-phosphoribosyl-1-pyrophosphate have been deposited with the Brookhaven Protein Data Bank under accession code 1OPR.

* Author to whom correspondence should be addressed [telephone (718) 430-2741; Fax (718) 597-5692].

[§] Albert Einstein Collge of Medicine.

[∥] Temple University Medical School.

[⊗] Abstract published in *Advance ACS Abstracts,* August 1, 1995.

[1] Abbreviations: OPRTase, orotate phosphoribosyltransferase; PRTase, phosphoribosyltransferase; HGPRTase, hypoxanthine−guanine phosphoribosyltransferase; Gln-aPRTase, glutamine-amidophosphoribosyltransferase; PRPP, α-D-5-phosphoribosyl-1-pyrophosphate; $PP_i$, pyrophosphate; OMP, orotidine 5′-monophosphate.

0006-2960/95/0434-10744$09.00/0 © 1995 American Chemical Society

enzyme's active site and documenting the nature of their interactions with enzyme atoms.

OPRTase is one of the smallest PRTases, consisting of 213 residues, and does not contain any known allosteric control sites. The *Salmonella typhimurium* enzyme has been sequenced (Scapin et al., 1993), overexpressed in *Escherichia coli*, and purified to homogeneity (Bhatia et al., 1990). Kinetic studies on *S. typhimurium* OPRTase (Bhatia et al., 1990) show that the enzyme follows a random sequential mechanism. Recently, the crystalline structure for OPRTase in complex with orotidine monophosphate (OMP; Scapin et al., 1994) has been reported. A surprising feature of this complex is that the two carboxylates of the conserved PRPP binding motif are not within hydrogen bond distance of any of the atoms of OMP (Scapin et al., 1994).

Two additional PRTase structures have been reported: the *Bacillus subtilis* glutamine-amido-PRTase (Gln-aPRTase; Smith et al., 1994), which contains two bound AMP molecules that are proposed to occupy the allosteric regulatory site and a site analogous to that of the product phosphoribosyl-1-amine; and the human hypoxanthine–guanine PRTase (HGPRTase; Eads et al., 1994) containing bound GMP. The three structures show a common fold for the domain responsible for PRTase activity, a five-stranded parallel twisted $\beta$-sheet surrounded by four $\alpha$-helices. The conserved PRPP binding motif also occupies a similar position in the three-dimensional structure of the three PRTases. This finding confirms the previous hypothesis (Musick, 1981; Scapin et al., 1994) that, like the NAD-binding enzymes, the PRTases have a common fold despite the lack of primary sequence similarity. In the OPRTase, Gln-aPRTase, and HGPRTase structures the 5′-phosphate of the bound product nucleotides occupies a similar position with respect to the nucleotide binding fold.

We report here the three-dimensional structure, solved and refined to 2.3 Å, of the complex of OPRTase with orotate and PRPP obtained by enzymatic reaction in the crystal. The position of the bound PRPP was confirmed by analysis of diffraction data to 2.1 Å collected from a crystal of apo-OPRTase soaked in PRPP.

## EXPERIMENTAL PROCEDURES

*Crystal Preparation.* Crystals of OPRTase without ligand and with bound OMP were obtained using the hanging drop vapor diffusion method as previously reported (Scapin et al., 1993). These crystals were tetragonal, space group $P4_12_12$, with unit cell parameters $a = b = 47.3$ Å and $c = 216.6$ Å. Crystals of the OPRTase·PRPP·orotate complex were obtained by adding a fresh solution of mother liquor containing 5 mM OMP, 5 mM $PP_i$, and 10 mM $MgCl_2$ to an OPRTase·OMP crystal. These crystals were subsequently analyzed using X-ray diffraction techniques. Crystals of the OPRTase·PRPP complex were produced by soaking apo-crystals in mother liquor containing 5.0 mM PRPP and 10.0 mM $MgCl_2$.

*Data Collection and Reduction.* The two data sets used in these studies were collected with a Siemens multiwire area detector equipped with a Rigaku RU-200 rotating anode X-ray source operating at 55 kV and 85 mA. Data for the OPRTase·PRPP·orotate complex were reduced using the Siemens package XENGEN (Siemens Analytical X-ray Instrument, Inc., Madison, WI) on a Silicon Graphics Iris computer. The $R_{sym}$ on intensities, for 12 880 reflections to 2.0 Å resolution (77.5% of the possible data), was 8.0%. Data collected from the OPRTase·PRPP complex were reduced using the program XDS (Kabsch, 1988). The resulting data set contained 11 164 reflections to 2.1 Å resolution (74% of the possible data), with an $R_{sym}$ on intensities of 4.8%. The two data sets were isomorphous ($a = b = 47.3$ Å and $c = 216.6$ Å for the OPRTase·PRPP·orotate complex, and $a = b = 47.3$ Å and $c = 217.0$ Å for the OPRTase·PRPP complex) with the OPRTase·OMP crystal. Table 1 summarizes statistics for data collection and reduction.

Table 1: Data Collection and Reduction

| | OPRTase·PRPP·orotate complex | OPRTase·PRPP complex |
|---|---|---|
| scan width (deg) | 0.25 | 0.25 |
| resolution range (Å) | 19.0–2.0 | 19.0–2.1 |
| no. of observations | 38356 | 33750 |
| mean $I/\sigma I$[a] | 19.3 | 18.1 |
| $R_{sym}$ on intensities | 8.0 | 4.8 |

| | no. of unique reflections | | % of possible | |
|---|---|---|---|---|
| lower resolution limit (Å) | PRPP·orotate complex | PRPP complex | PRPP·orotate complex | PRPP complex |
| 3.71 | 2921 | 2475 | 97.5 | 82.8 |
| 2.94 | 2453 | 2241 | 88.2 | 80.3 |
| 2.57 | 2231 | 2433 | 81.2 | 88.8 |
| 2.33 | 2164 | 2270 | 79.5 | 83.1 |
| 2.17 | 1929 | 1745 | 67.4 | 64.4 |
| 2.03 | 1182 | | 44.5 | |
| total | 12880 | 11164 | 77.5 | 73.6 |

[a] $I$ is defined as average intensity for all scaled observations of a reflection.

*Structure Refinement.* A model of native OPRTase without bound OMP and solvent molecules was initially used to phase the data set collected from the OPRTase·PRPP·orotate complex. Fifty cycles of rigid body refinement were initially run (using X-PLOR; Brunger et al., 1987), followed by the simulated annealing procedure "slowcool" described in the X-PLOR manual (Brunger, 1992). Both steps were run using data between 15.0 and 2.6 Å resolution, applying a $2\sigma$ cutoff. At the end of this first step, the $R$-factor was 22.5%. Cycles of manual rebuilding and computer-based least squares refinement (TNT; Tronrud et al., 1987) were subsequently used to improve the model and to extend the resolution to 2.4 Å. Forty-eight solvent molecules were added to the model, to account for positive peaks in $[(F_o - F_c)\phi_{calc}]$ electron density maps that were greater or equal to three times the standard deviation of the electron density map. The resulting crystallographic $R$-factor was 20.2%, with an rms deviation for bond lengths and bond angles of 0.024 Å and 2.9°, respectively. At this point, inspection of $[(F_o - F_c)\phi_{calc}]$ difference electron density maps (contoured at $3\sigma$) in the area corresponding to the active site of the protein clearly revealed the presence of two areas of positive electron density that could not be attributed to protein atoms. These positive electron densities were localized in two distinct regions of the active site, about 6 Å apart and without any evident connection between them. Orotate and PRPP were built into these regions of electron density. All the subsequent cycles of refinement were carried out using TNT (Tronrud et al., 1988) and including the two substrates in the structure. The final crystallographic $R$-factor, for 8993 reflections with

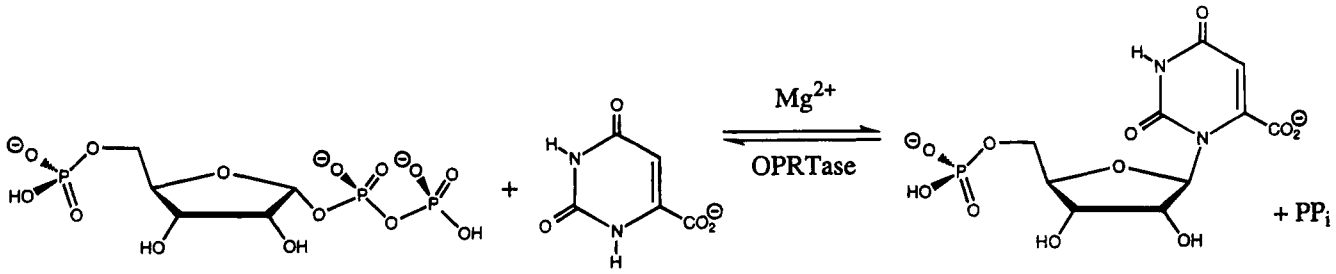


FIGURE 1: Scheme of the reaction catalyzed by orotate phosphoribosyltransferase.

intensities greater than $2\sigma$ (76% of the possible data) between 15.0 and 2.3 Å, is 18.7%, with rms deviations for bond lengths and bond angles of 0.017 Å and 2.5°, respectively. The refined model without PRPP and orotate was then used to run 60 cycles of TNT refinement against the data set collected from the OPRTase•PRPP complex. A total of 8443 reflections (with a $2\sigma$ cutoff on intensities, 72% of the possible data) between 15.0 and 2.3 Å were used. The resulting $R$-factor was 19.8%, and the structure maintained good geometry (rms deviations for bond lengths and bond angles were 0.021 Å and 2.7°, respectively). Inspection of a $[(F_o - F_c)\phi_{calc}]$ difference Fourier map (contoured at $3\sigma$) contained positive electron density in the area corresponding to the PRPP molecule found in the OPRTase•PRPP•orotate complex. An α-PRPP molecule was then included in the model. An additional 60 cycles of TNT refinement yielded a structure with a conventional $R$-factor of 17.9%, with rms deviations for bond lengths and bond angles of 0.019 Å and 2.4°, respectively, using data in the range 15.0−2.3 Å.

## RESULTS AND DISCUSSION

*Crystal Complex Preparation.* The crystalline OPRTase•PRPP•orotate complex was obtained by carrying out the enzymatic reaction in the OMP-containing crystals. Figure 1 shows the reaction catalyzed by OPRTase. Kinetic studies of the OPRTase from *S. typhimurium* showed that the reaction proceeds via a random sequential mechanism (Bhatia et al., 1990). A $K_{eq}$ of 0.1 (Bhatia et al., 1990) favors the reverse reaction, that is, the production of PRPP and orotate. In order to form this complex, crystals of OPRTase with bound OMP were transferred to a freshly made solution containing OMP and $PP_i$ (as described under Experimental Procedures). The subsequent addition of $Mg^{2+}$ activated the enzyme to promote the thermodynamically favored ($K_{eq}$ is 0.1) reverse reaction (Figure 1), resulting in the production of orotate and PRPP. The presence of PRPP and orotate was evident in $[(|F_o| - |F_c|)\phi_{calc}]$ difference Fourier electron density maps (Figure 2a). In order to further confirm the position of the binding site for PRPP, X-ray diffraction data were collected from a OPRTase crystal soaked in PRPP. This complex was obtained by soaking crystals of apo-OPRTase (i.e., a crystal of OPRTase without any bound substrate) in a solution containing PRPP and $Mg^{2+}$. Difference Fourier maps $[(|F_o| - |F_c|)\phi_{calc}]$, calculated as described under Experimental Procedures, clearly showed electron density corresponding to a PRPP molecule in the same position as found in the OPRTase•PRPP•orotate complex but lacked the orotate molecule (Figure 2b). No further refinement was carried out on this complex.

*Quality of the Structure.* The refined structure of the OPRTase•PRPP•orotate complex contains 1644 of 1660 non-hydrogen protein atoms (Glu101, Asp104, His105, and Glu107 were included without side chains, i.e., as alanine residues), 60 solvent molecules, and the two substrates, orotate and PRPP. The coordinates have a conventional $R$-factor of 18.7%, using data between 15.0 and 2.3 Å resolution with intensities greater than $2\sigma$ (76% of the possible data). The rms deviations of the bond lengths and bond angles from ideality for the final model are 0.017 Å and 2.5°, respectively. A Ramachandran plot of the Φ,Ψ angles of the OPRTase backbone, as calculated with the program PROCHECK (Laskowski et al., 1993) shows that all but three of the non-glycine residues are in the allowed areas of low energy. Of these three residues, Ala104 and Ser110 are located in a long and flexible loop (Asn98−Arg119) and are characterized by poor electron density. The third residue (Ala71) is in a turn which may be important for ligand binding.

The mean temperature factor for main-chain atoms of the OPRTase•PRPP•orotate complex is 33.9 Å$^2$. For side-chain atoms, the mean temperature factor is 35.7 Å$^2$. Temperature factors greater than 50.0 Å$^2$ are associated with residues located in the flexible surface loop and side-chain atoms of surface residues, such as lysines, arginines, and glutamic acids.

*Overall Structure.* The OPRTase•PRPP•orotate and OPRTase•PRPP crystals are isomorphous with the OPRTase•OMP crystals originally used to solve the OPRTase structure. The fold of the OPRTase•PRPP•orotate complex closely resembles the one of the OPRTase•OMP complex (Scapin et al., 1994). The protein contains 213 residues arranged in a single domain, of about 51 × 33 × 27 Å. Figure 4 is a ribbon diagram of OPRTase, and Table 2 summarizes the protein secondary structure elements. The protein can be divided into three regions: (i) an N-terminal region spanning residues 1−37[2] and containing three short antiparallel β-strands which we refer to as the "hood" (Scapin et al., 1994), (ii) a core region (residues 41−181) that shows a topology similar to the dinucleotide binding fold found in many dehydrogenases [Rossmann et al., 1975; for a review, see Branden and Tooze (1991)], and (iii) a C-terminal region (residues 185−213) containing two antiparallel α-helices (A6 and A7, Figure 3) connected by a short loop. The core contains a five-stranded twisted β-sheet (B1 through B5; see Figure 3) surrounded by four α-helices (A2 through A5). α-Helix A6 runs perpendicular to A1 of the N-terminal hood,

[2] In our previous paper (Scapin et al., 1994) we defined the N-terminal region as spanning residues 1−60. Comparison of the OPRTase structure with the recently reported structures of HGPRtase (Eads et al., 1994) and Gln-aPRTase (Smith et al., 1994) reveals that α-helix A2 (Asn 41−Val58 in OPRTase) is present in all three structures and thus belongs to the conserved core rather than to the N-terminal region.

FIGURE 2: Stereo diagram of difference Fourier electron density maps for the (a, top) OPRTase•PRPP•OMP complex and (b, bottom) OPRTase•PRPP complex. The maps were calculated without including substrates and water molecules in the model.

and the C-terminal end of A7 (residues 200−207) is packed against residues 29−33 of the hood. This arrangement has been proposed to serve in stabilizing the conformation of the hood region (Scapin et al., 1994). With the exception of residues Lys103−Glu107, all three regions of the protein appear to be well ordered in the electron density map, as indicated by their relatively low temperature factors. Residues 102−110, located in a surface loop (Asp98−Arg119) connecting the two halves of the core $\alpha/\beta$ region displayed poor electron density throughout the refinement procedure. Amino acids Ala102−Lys103 and Gly106−Ser110 could only be fit in the final stage of refinement using unbiased omit electron density maps (maps calculated excluding residues Lys100−Leu111 from the final refinement and the structure factor calculation), while no clear density was observed for Asp104 and His105. The very high temperature factors found for atoms of this region (60−90 Å$^2$) and the poor electron density associated with this area indicate that the loop is flexible in the crystal structure. Nevertheless, the side chains of Arg99, Lys100, and Lys103 could be unambiguously fitted. Previous work has shown that residues of this loop appear to play a role in catalysis. For example, Lys103 has been shown by both chemical modification (Bhatia & Grubmeyer, 1993) and mutation studies (following papers in this issue) to be essential for enzyme activity. The presence of this residue, along with the disorder of the whole region, suggests that loop movement is a component of the catalytic mechanism.

OPRTase functions as a dimer in solution (Bhatia et al., 1990; Ozturk et al., 1995a,b). Our previous analysis of the crystal packing of OPRTase in the $P4_12_12$ space group (Scapin et al., 1994) revealed that the dimer was formed along a crystallographic 2-fold axis. The orientation of the two subunits was such that the two active sites of the dimer were in close proximity to one another. An identical dimer is found in the OPRTase•PRPP•orotate complex. The distance between the pyrophosphate moiety of PRPP in the two binding sites is about 16 Å (Figure 4). The two subunits

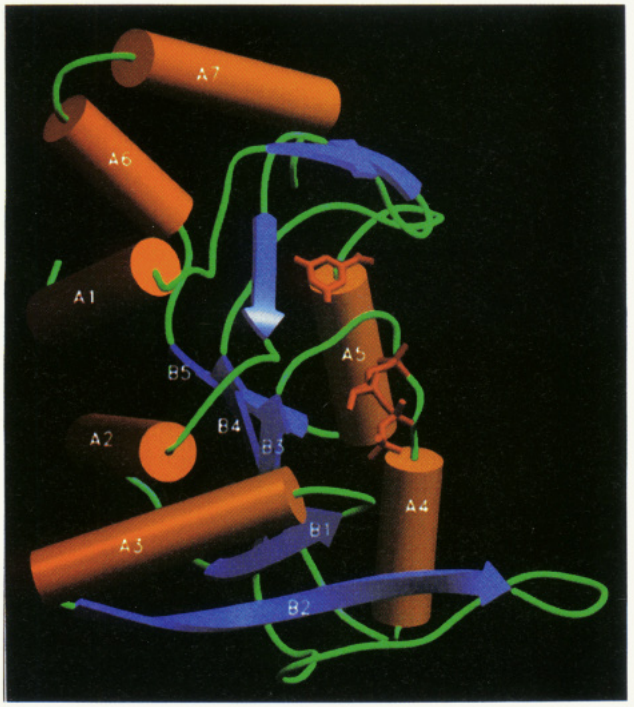


FIGURE 3: Ribbon diagram of the three-dimensional structure of *S. typhimurium* OPRTase. The two bound substrates (orotate and PRPP) are shown as stick representation. For a complete description of the secondary structure elements of OPRTase, see Table 2. This figure was generated with the program SETOR (Evans, 1993).

Table 2: Secondary Structure Elements of OPRTase

| residues involved | secondary structure | name (as in Figure 3) |
|---|---|---|
| Met1−Leu13 | α-helix | A1 |
| Gly21−Thr24 | β-strand | |
| Gly28−Ser31 | β-strand | |
| Tyr33−Ala37 | β-strand | |
| Asn41−Val58 | α-helix | A2 |
| Leu66−Ala71 | β-strand | B1 |
| Gly74−Glu87 | α-helix | A3 |
| Lys91−Phe97 | β-strand | B2 |
| Val120−Asp125 | β-strand | |
| Arg134−Gln141 | α-helix | A4 |
| Leu147−Ile152 | β-strand | B4 |
| Ser165−Asp173 | α-helix | A5 |
| Cys176−Ile181 | β-strand | B5 |
| Lys185−Glu192 | α-helix | A6 |
| Met197−Glu210 | α-helix | A7 |

interact through three regions, α-helix A3 (defined in Table 2), the loop region before α-helix A2, and β-strand B2. The interface surface area buried by the dimer is about 1100 Å$^2$ (12% of the total monomer surface) of which 35% is hydrophobic, 24% polar, and 41% ionizable. The Asn98−Arg119 loops of each subunit are also located at the interface in close proximity to the two active sites of the dimer (Figure 4).

*Binding Site.* In the OPRTase•OMP structure, OMP was located at the C-terminal end (as seen in Figure 4) of the five-stranded β-sheet that constitutes the core of the protein. The orotate moiety was located between the N-terminal hood and the α/β core of the protein: this location now appears to be a determinant of base specificity among the three PRTases with known three-dimensional structures (Scapin et al., 1994; Smith et al., 1994; Eads et al., 1994). Most of the interactions between the base and the protein involve protein main-chain atoms (see Table 3a), as found for HGPRTase (Eads et al., 1994). The ribose of OMP was found in a solvent-exposed region of the binding site, making only few interactions with protein atoms (see Table 3a). The 5′-phosphate forms an extended network of hydrogen bonds with main-chain and side-chain atoms of the amino acids comprising the C-terminal portion of the PRPP binding motif (that spans Val120−Thr131 in OPRTase), which we refer to as the phosphate binding loop. Unexpectedly, no direct hydrogen bonds were identified between the bound OMP and the two conserved aspartic acids of the proposed PRPP binding motif (Asp124 and Asp125) in the OPRTase•OMP crystal structure.

In the OPRTase•PRPP•orotate complex, two regions of strong density in difference Fourier electron density maps

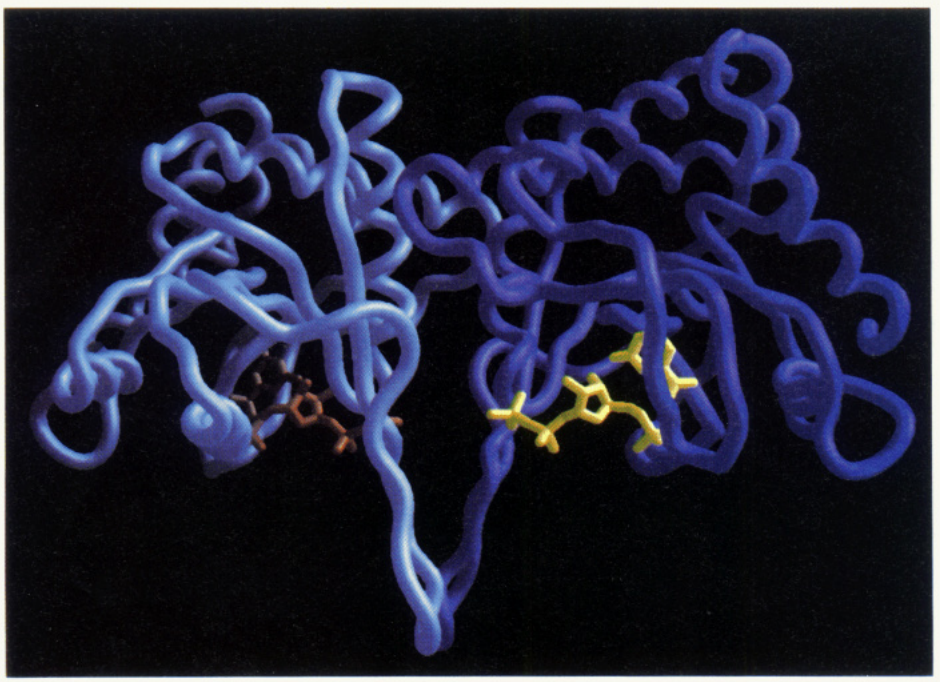

FIGURE 4: Ribbon representation of the OPRTase dimer. The two binding sites are evidenced by the presence of the two bound substrates. This figure and Figure 6a were generated using the program GRASP (Nichols, 1991).

Table 3: Interactions of Bound OMP and Bound Orotate/PRPP with OPRTase[a]

(a) Bound OMP with OPRTase

| | possible hydrogen bond interactions | | van der Waals contacts | | | possible hydrogen bond interactions | | van der Waals contacts | |
|---|---|---|---|---|---|---|---|---|---|
| OMP atom | protein atom | distance (Å) | protein atom | distance (Å) | OMP atom | protein atom | distance (Å) | protein atom | distance (Å) |
| orotate ring | | | | | ribose ring | | | | |
| N1 | | | CZ Phe34 | 4.0 | O2′ | | | CZ Phe34 | 2.9 |
| C2 | | | CE Phe34 | 4.4 | O3′ | NZ Lys26 | 3.2 | | |
| O2 | | | O Phe35 | 3.3 | O4′ | Oγ1 Thr128 | 3.3 | | |
| | | | Cγ1 Val126 | | | | | Cγ2 Thr128 | |
| N3 | O Phe35 | 3.2 | | | O5′ | | | O Val126 | 2.8 |
| C4 | | | Cγ Phe34 | 4.5 | 5′-phosphate | | | | |
| O4 | NH1 Arg156 | 2.5 | | | OP1 | Oγ1 Thr128 | 3.2 | | |
| | NE Arg156 | 2.9 | | | | N Ala129 | 3.2 | | |
| | | | Cδ Arg156 | 2.5 | | Oγ1 Thr131 | 3.1 | | |
| | | | Cγ Arg156 | 3.1 | | | | Cγ2 Thr131 | 3.3 |
| | | | CZ Arg156 | 3.0 | OP2 | O Val126 | 3.2 | | |
| | | | N Phe 35 | 3.9 | | N Thr128 | 2.9 | | |
| C6 | | | CE2 Phe34 | 4.1 | | Oγ1 Thr131 | 2.6 | | |
| O71 | N Lys26 | 3.1 | | | | | | Cγ2 Ile127 | 3.4 |
| | | | Cβ Ile25 | 3.4 | OP3 | NZ Lys73 | 3.4 | | |
| | | | Cβ Lys26 | 3.5 | | | | | |
| O72 | | | Cγ2 Thr128 | 2.9 | | | | | |
| | | | Cβ Thr128 | 3.1 | | | | | |

(b) Bound Orotate/PRPP with OPRTase

| | possible hydrogen bond interactions | | van der Waals contacts | | | possible hydrogen bond interactions | | van der Waals contacts | |
|---|---|---|---|---|---|---|---|---|---|
| orotate/PRPP atom | protein atom | distance (Å) | protein atom | distance (Å) | orotate/PRPP atom | protein atom | distance (Å) | protein atom | distance (Å) |
| orotate | | | | | PRPP-ribose | | | | |
| N1 | | | CZ Phe34 | 3.6 | O1′ | $Mg^{2+}$ | 2.6 | | |
| C2 | | | CE Phe34 | 4.0 | O2′ | NZ Lys73 | 3.2 | | |
| O2 | | | O Phe35 | 3.3 | | $Mg^{2+}$ | 2.6 | | |
| N3 | O Phe35 | 2.7 | | | | | | Cβ Lys73 | 3.2 |
| | | | Cδ1 Phe34 | 4.4 | O3′ | $Mg^{2+}$ | 2.7 | | |
| C4 | | | Cγ Phe34 | 4.3 | | Oδ1 Asp124 | 3.4 | | |
| O4 | N Phe35 | 3.0 | | | | Oδ2 Asp124 | 3.0 | | |
| | NH1 Arg156 | 3.2 | | | O4′ | Wat555 | 2.8 | | |
| | | | Cβ Phe35 | 3.4 | C5′ | | | Wat555 | 3.3 |
| | | | Cδ Arg156 | 3.4 | PRPP-pyrophosphate | | | | |
| C5 | | | CE2 Phe34 | 3.4 | O | $Mg^{2+}$ | 2.6 | | |
| | | | Cδ2 Phe34 | 3.8 | O6 (β-phosphate) | NZ Lys73 | 3.4 | | |
| C6 | | | CE2 Phe34 | 3.5 | | NE Arg99# [b] | 3.1 | | |
| O71 | Wat357 | 3.0 | | | | NH2 Arg99# | 2.3 | | |
| | N Lys26 | 3.1 | | | | | | CE Lys73 | 2.9 |
| | | | Cβ Lys26 | 3.5 | | NE Arg99# | 3.4 | | |
| O72 | Wat508 | 2.8 | | | O7 (β-phosphate) | NZ Lys100 | 2.8 | | |
| | Wat559 | 2.6 | | | | NE Arg99# | 3.4 | | |
| PRPP-5-phosphate | | | | | | $Mg^{2+}$ | 2.8 | | |
| O1 | N Thr128 | 3.2 | | | O8 (β-phosphate) | N Phe72 | 2.7 | | |
| | N Ala129 | 3.3 | | | | N Lys73 | 2.3 | | |
| | N Gly130 | 3.0 | | | | | | C Phe72 | 3.1 |
| O2 | N Thr131 | 3.4 | | | | | | Cα Phe72 | 2.9 |
| | Oγ1 Thr131 | 3.2 | | | | | | Cβ Phe72 | 2.9 |
| | N Ala132 | 2.9 | | | | | | | |
| | | | Cβ Ala132 | 3.3 | | | | | |
| O3 | Oγ1 Thr128 | 2.7 | | | | | | | |
| | N Ala129 | 3.1 | | | | | | | |
| | | | Cβ Ala129 | 3.1 | | | | | |
| | | | NZ Lys126 | 3.5 | | | | | |

[a] The hydrogen bond cutoff was set to 3.5 Å for bound substrates with OPRTase. [b] # indicates a residue from the symmetry-related molecule.

(Figure 2a) allowed us to position the two substrates. Table 3b summarizes the interactions between the substrates and the protein. The first peak of electron density was disk shaped and located under the hood. This density occupies a location nearly identical to that of the orotate base of OMP (Scapin et al., 1994). The orotate ring (Figure 5) is parallel and stacked with the phenyl ring of Phe35; its O4 hydrogen bonds to the main-chain nitrogen of Phe35 and to a guanidinium nitrogen of Arg156. The N3 atom of orotate hydrogen bonds to the main-chain oxygen of Phe35, and the carboxylate hydrogen bonds to the main-chain nitrogen of Lys26 and three ordered water molecules located in the binding site.

The second region of contiguous positive $[(|F_o| - |F_c|)\phi_{calc}]$ electron density was also located in the active site, in a cavity formed by the loops between β-strand B2 and α-helix A3, and B3/A4 (Figure 2a). The density was about 11 Å long, which corresponds well to the size of a PRPP molecule. In

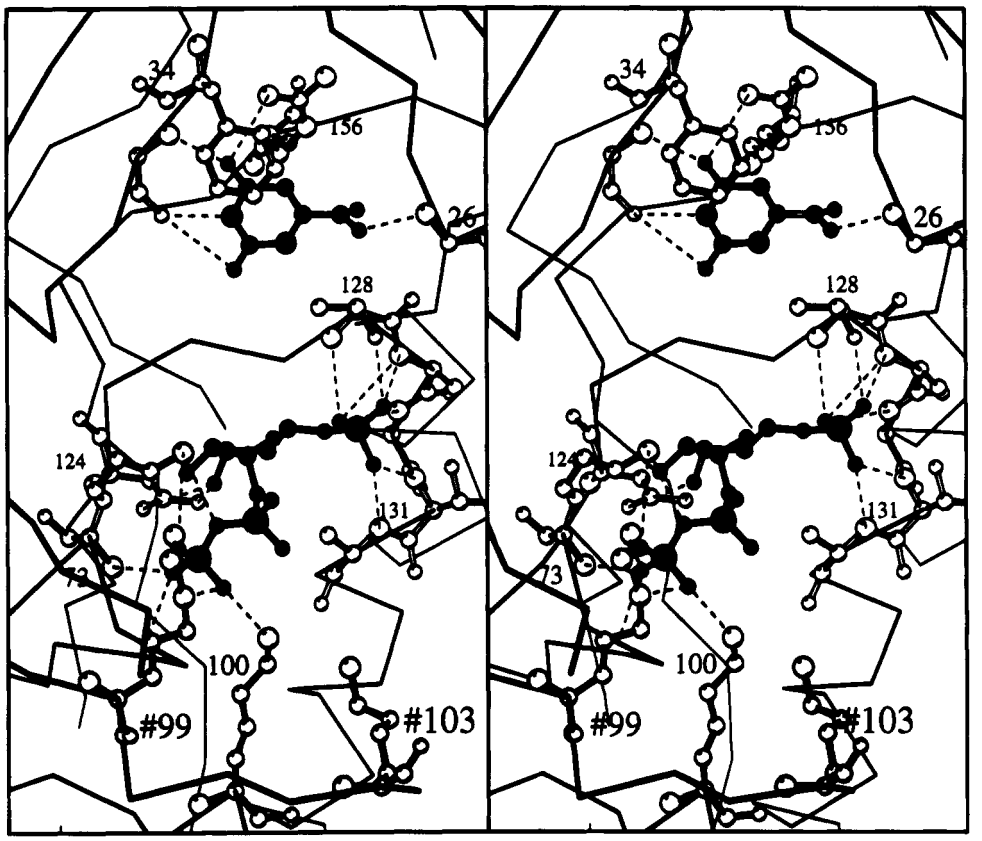


FIGURE 5: Stereo diagram of the *S. typhimurium* OPRTase binding site. Dashed lines represent the interactions of orotate and PRPP with the protein. The OMP moiety was omitted for clarity. This figure and Figures 6b, 7, and 8 were generated with the program MOLSCRIPT (Kraulis, 1991).

order to confirm that this density was in fact PRPP, an X-ray diffraction data set was collected from crystals of apo-OPRTase incubated in presence of PRPP and $Mg^{2+}$. Difference electron density maps for the two complexes were identical in this region (Figure 2). A molecule of α-PRPP was thus modeled into the electron density. The three oxygens of the 5′-phosphate form an extensive network of hydrogen bonds with main-chain and side-chain atoms of residues of the conserved PRPP binding motif (Figure 6 and Table 3b). The ribose is in the 2′-endo conformation (Figure 6) with its O3′ hydroxyl group hydrogen bonding to the conserved Asp124 of the PRPP binding motif. O2′ is hydrogen bonded to the side-chain nitrogen of Lys73. The pyrophosphate extends toward the dimer interface where the β-phosphate oxygen atoms interact with the side-chain nitrogens of Lys73 and Lys100 and the main-chain nitrogens of Phe72 and Lys73 from the same subunit, and with the guanidinium group of Arg99# from the other subunit of the dimer.

Six additional peaks of strong electron density were identified in the binding site during the refinement procedure. One of these peaks was fit as the $Mg^{2+}$ ion required for catalysis. This assignment was based on the position of this peak and on the number of hydrogen bonds (six) it could form, both similar to what is reported for other $Mg^{2+}$ binding proteins (see below). The other five peaks were fit as ordered water molecules. Comparable electron density for all six peaks was found in the diffraction data collected from the MgPRPP soaked crystal. Previous studies have shown that $Mg^{2+}$ when bound to a protein is typically coordinated in an octahedral arrangement (Hurley et al., 1991; Murphy et al., 1993). In many $Mg^{2+}$ binding enzymes, a magnesium binding motif has been identified from sequence comparison (Black & Hruby, 1992): in its simplest version, it reads Xh Xh Xh Xh D, where Xh is any hydrophobic residue. The four hydrophobic residues generally form a β-strand, and the key residue in the binding is the aspartic acid, which lies at the end of the β-strand. The $Mg^{2+}$ ion usually interacts directly with this aspartic acid residue (Hurley et al., 1991; Green et al., 1993), but indirect interactions, mediated by water molecules, have also been reported (Harmak et al., 1992). In OPRTase, the magnesium ion binding motif may be represented by residues $^{120}$VMLVD$^{124}$ of β-strand B3. The $Mg^{2+}$ ion is bound in a nearly octahedral coordination: three of the six interactions involve oxygens of the pyrophosphate moiety (2.9, 2.6, and 2.8 Å), and the remaining three involve the two ribose hydroxyls (2.5 and 2.7 Å) and an ordered water molecule (2.6 Å). This water is in turn bound to the carboxylate of Asp124 and the main-chain nitrogens of Lys73 and Gly74. Thus, in the OPRTase three-dimensional structure, $Mg^{2+}$ appears to interact indirectly with atoms of the protein, via an intermediate ordered water. This is in accord with previously reported studies on the role of $Mg^{2+}$ in activating the OPRTase reaction (Bhatia & Grubmeyer, 1993). In that paper, the authors concluded from kinetic and spectroscopic studies that the metal forms a MgPRPP complex that then serves as substrate for the OPRTase reaction. No tight binding (<50.0 μM) of metal ion with the protein was detected.

The arrangement of the subunit of the dimer found for the OPRTase·PRPP·orotate complex is identical to that in the OPRTase·OMP complex. This arrangement positions the

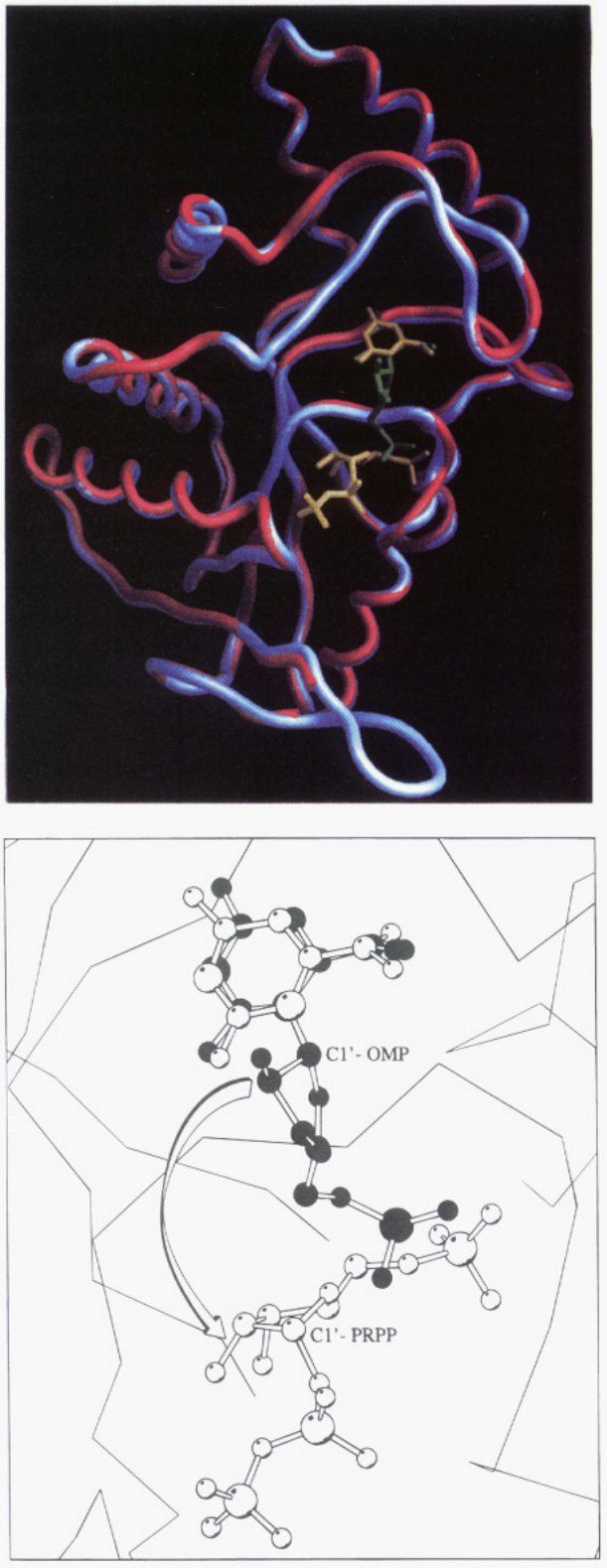


FIGURE 6: (a, top) Superimposition of the Cα trace for OPRTase•OMP (orange) and OPRTase•PRPP•orotate (light blue) complexes. OMP (green) and orotate and PRPP (yellow) are also shown. (b, bottom) Schematic representation of the movement the ribose ring undergoes when the OMP and orotate•PRPP structures are compared.

active sites of each subunit in close proximity. In fact, the side chains of several residues near the active site of one subunit are available to the adjacent subunit's active site. In our previous work (Scapin et al., 1994) we proposed that the side chains of conserved basic residues from a flexible surface loop at the interface of the two active sites, specifically Arg99, Lys100, and Lys103, were involved in the binding of pyrophosphate. Analysis of the PRPP binding site in the three-dimensional structure of the OPRTase•PRPP•orotate complex shows that Lys100 and Lys73 from one subunit and Arg99 from the other subunit of the dimer interact with the bound PRPP. Lys103 is also located nearby, with its side chain facing toward the PRPP binding site of the neighboring molecule. These observations confirm our previous hypothesis and suggest that a dimer is required for catalysis. Chemical modification (Grubmeyer et al., 1993) and mutational (Ozturk et al., 1995a,b) studies also showed that Lys100 and Lys103 were involved in interactions with pyrophosphate and that Lys103 is essential for catalysis but exercises its role in the adjacent active site. In our three-dimensional structure the side-chain nitrogen of Lys103 is about 6 Å away from the pyrophosphate moiety of bound PRPP, and it appears that it has to move closer to the active site in order to participate in catalysis. The assumption of a very large degree of flexibility for Lys103 as well as several other residues of this loop could explain the absence of well-ordered electron density and the high temperature factors found for atoms of this region.

*Comparison of the OPRTase•Substrate Complexes.* Figure 6a shows a superimposition of OMP and orotate•PRPP in the OPRTase active site. The protein maintains a similar overall structure in the two complexes, with an rms difference (for all protein atoms) of about 0.6 Å. The orotate and the orotate ring of OMP also occupy nearly identical positions, although the position occupied by orotate in the OPRTase•PRPP•orotate complex allows the formation of slightly more favorable van der Waals and hydrogen-bonding interactions with atoms of the protein (see Table 3). The position of the phosphoribosyl moiety is quite different in the OMP and PRPP•orotate complexes, varying by up to 10 Å for equivalent atoms. In both complexes, the 5′-phosphate is located in the phosphate binding loop (residues 128−132); however, in the PRPP-containing complex it is shifted by 1.7 Å toward the center of the loop, if compared to its position in the OPRTase•OMP complex. This slight repositioning does not change the number of hydrogen bonds formed between the 5′-phosphate and atoms of the protein, but while in the OPRTase•OMP complex one hydrogen bond is formed with the side-chain nitrogen of Lys73, in the OPRTase•PRPP•orotate complex they all involve only main- and side-chain atoms of residues in the phosphate binding loop (Ile127−Ala132) (see Table 3). The largest difference in position between the substrates occurs at the ribose group. The ribose in the PRPP-containing complex is translocated across the binding cavity when compared to the ribose of bound OMP. Superpositioning of the ribose of OMP onto that of PRPP requires a rotation of about 60° around the pivot of the phosphate group and a twist of about 180° with respect to the enzyme (Figure 6b). As a result, the ribose C1′ is located about 7 Å away from its position in the OMP-containing complex. The number of interactions between the ribose atom and the proteins is increased in the PRPP complex. In the OPRTase•OMP complex the ribose hydroxyl O3′ forms only one weak hydrogen bond with the side-chain nitrogen of Lys26 (Table 3a). In the OPRTase•PRPP•orotate complex there are five hydrogen-bonding interactions involving the ribose O2′ and O3′, three with atoms of residues

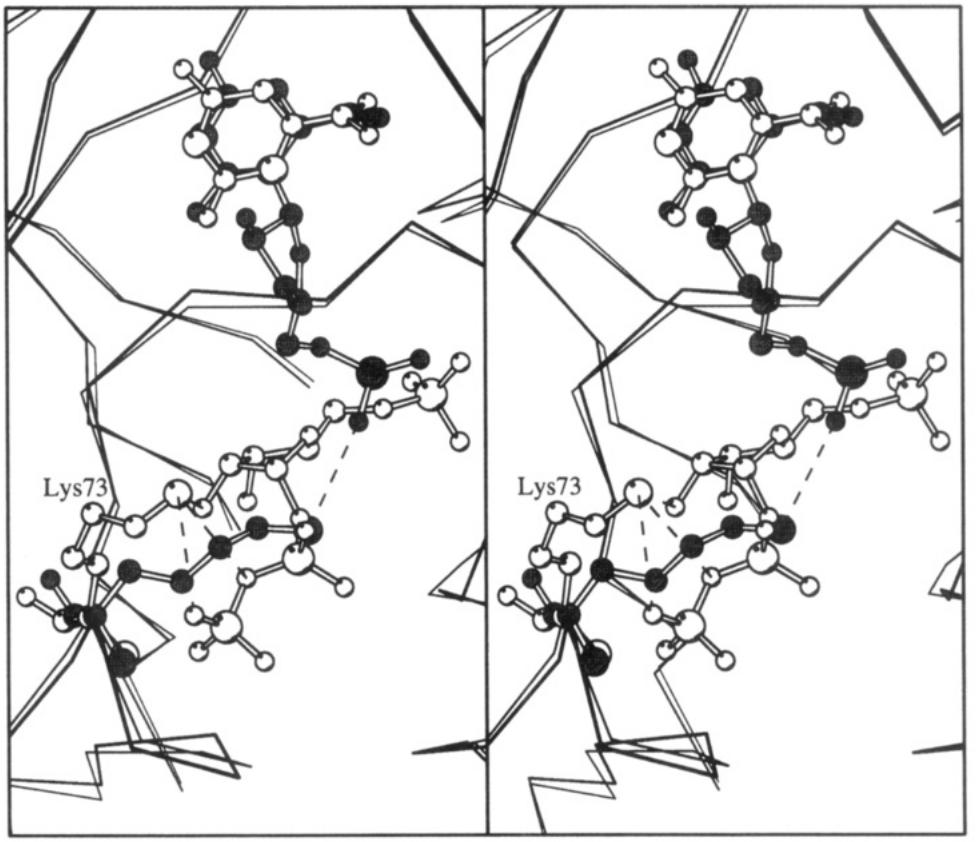


FIGURE 7: Comparison between the position of the side chain of Lys73 in the OPRTase•OMP complex (●) and in the OPRTase•PRPP•orotate complex (○).

Lys73 and Asp124 (NZ of Lys73 and Oδ1 and Oδ2 of Asp124) and two with the $Mg^{2+}$ ion (Table 3b). The location of the ribose in the OPRTase•PRPP•orotate complex is similar to that found for the ribose in Gln-aPRTase (the ribose of the AMP that has been proposed to occupy the site of the product phosphoribosyl-1-amine; Smith et al., 1994) and in GMP-liganded HGPRTase (Eads et al., 1994).

Differences in the bound substrates are reflected only slightly in the overall structure of OPRTase. The protein backbone structure of the two complexes appears to be very similar (Figure 6a). A superimposition of the Cα trace for the two models yielded an overall rms difference of 0.44 Å, with the largest differences occurring in three discrete regions defined by the turn between β-strand B2 and α-helix A3 (residues Ala71−Gly74), the long extended loop between the first and the second half of the core α/β motif (residues Asn98−Arg119), and the C-terminal portion of the conserved PRPP binding motif (residues Ile127−Ala132). While the differences found in the long loop may be attributable to lack of order in both complexes, the differences found in the other two regions are a result of the differences in binding between the protein and substrates.

The movement observed for residues Ala71−Gly74 appears to result from the presence of the pyrophosphate group of PRPP. The side chain of Lys73 (Figure 7) extends across the binding cavity to form a hydrogen bond to the 5′-phosphate moiety of OMP. In the PRPP•orotate complex, this side chain is shifted away from the binding cavity, toward the N-terminal portion of α-helix A2. This repositioning is necessary to allow the binding of the pyrophosphate moiety of PRPP. In the OMP complex the ϵ-amino group of Lys73 hydrogen bonds the OMP 5′-phosphate, whereas in the PRPP•orotate complex it hydrogen bonds with the O2′ of the ribose ring and the β-phosphate of PRPP. Lys68 of HGPRTase (Eads et al., 1994) occupies a position similar to that of Lys73 in the OPRTase•PRPP•orotate complex, in close proximity to the nucleotide. The phosphate binding loop (residues Ile127−Ala132), located at the C-terminal region of the PRPP binding motif, is also affected by the presence of different substrates. When the two loops are superimposed, there is a rms difference between their Cα atoms of about 0.8 Å. As shown in Figure 8, this difference is mainly due to the conformational movement of the Gly130−Thr131 dipeptide, required in order to maintain the hydrogen bond interactions with the shifted 5′-phosphate, described above.

*Conclusions.* The reaction catalyzed by OPRTase proceeds with inversion of the stereochemistry at the anomeric carbon (Chelsky & Parson, 1975). A $S_N1$-like mechanism (Goitein et al., 1978) with a loosely associative oxocarbonium-like transition state for phosphoribosyl transfer has been proposed (Bhatia et al., 1990). The generation of the oxocarbonium ion would be achieved by breaking the C1′−O1′ bond of the PRPP molecule in the direct reaction (Figure 1) or the C1′−N1 bond in OMP in the reverse reaction. From a comparison between the two available OPRTase three-dimensional structures, it appears that the C1′ of the ribose has to move about 7 Å across the active site (Figure 7). Both orotate and $PP_i$ binding sites have been reasonably established on the basis of crystallographic (present work) and kinetic and mutational studies (Ozturk et al., 1995a). The orotate binding site is located under the hood, and the $PP_i$ binding site is presumably located where the pyrophosphate moiety of PRPP is bound. The relative position of these

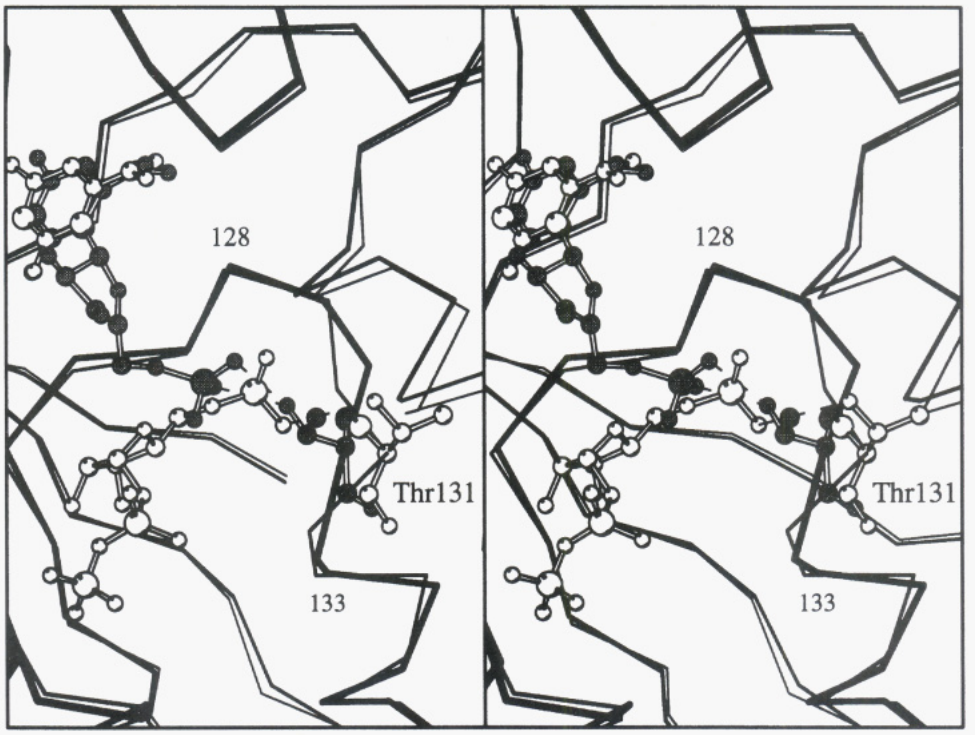


FIGURE 8: Comparison between the conformation of the Val127−Ala133 loop in the OPRTase•OMP complex (thicker line, ●) and in the OPRTase•PRPP•orotate complex (thinner line, ○).

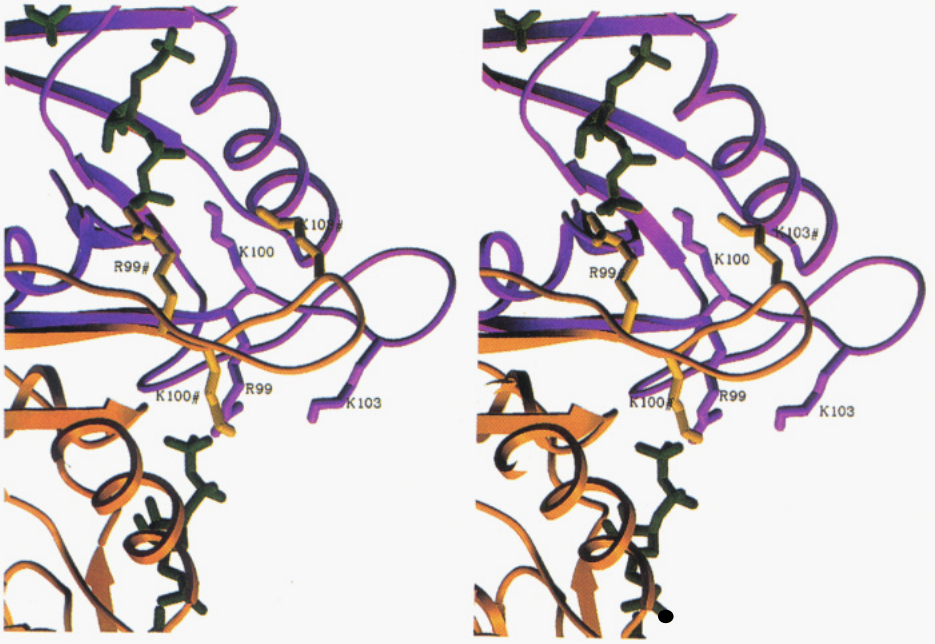


FIGURE 9: Stereoview of the OPRTase dimer active sites showing the two flexible loops and the residues involved in substrate binding.

two binding sites would imply a swinging movement of the C1′-oxocarbonium across the cavity in order to move from one ground state to the other. Analysis of the solvent accessibility for the OPRTase binding site strongly opposes this long movement of the reactive carbonium atom. The solvent accessibility calculation of the bound substrates in the PRPP complex (Insight, Biosym Inc., San Diego, CA; the probe radius used in the calculation was 1.4 Å) shows that about half of the PRPP surface (145 Å$^2$ out of 305 Å$^2$), including the C1′, and a third of the orotate surface (47 Å$^2$ out of 150 Å$^2$) are solvent accessible. Therefore, for the reaction to proceed via an oxocarbonium ion, it will be essential to close the active site to exterior water molecules which could react with the nascent oxocarbonium ion. Conformational adjustments of the protein would be necessary in order to shield the active site during the transition state. One of these conformational movements could involve the surface loop spanning residues Asn98−Arg119, which contains Lys103. Lys103 has been shown to be important for catalysis, although the nature of its involvement is not yet clear (Ozturk et al., 1995a,b). In our model Lys103 is somewhat (about 6 Å) distant from the active site, and the loop to which it belongs appears to be flexibile. A movement of this loop would serve not only to position the side chain of Lys103 closer to the active site but would close the active site to solvent.

The loop that we propose to be involved in active site desolvation is in one subunit directly adjacent to the loop

and active site of the second subunit of the dimer (Figure 9). Since at least one of the residues of the loop (Lys100) interacts with the substrate in its own subunit and at least one residue of the same loop (Arg99) interacts with the neighboring subunits substrate, we propose that there is an asymmetry in catalysis, in which catalysis would proceed alternatively in the two active sites. The structure of OPRTase in complex with a transition-state analog, or with a substrate capable of holding either loop in a "closed" conformation, would be useful to confirm this proposed mechanism.

## REFERENCES


Bhatia, M. B., & Grubmeyer, C. (1993) *Arch. Biochem. Biophys. 303*, 321−325.

Bhatia, M. B., Vinitsky, A., & Grubmeyer, C. (1990) *Biochemistry 29*, 10480−10487.

Black, M. E., & Hruby, D. E. (1992) *J. Biol Chem. 267*, 6801−6806.

Branden, C., & Tooze, J. (1991) *Introduction to protein structure*, Garland Publishing, Inc., New York, NY.

Brünger, A. T. (1992) *X-PLOR Version 3.0 Manual: a System for Crystallography and NMR*, Yale University, New Haven, CT.

Brünger, A. T., Kuryan, J., & Karplus, M. (1987) *Science 223*, 458−460.

Chelsky, D., & Parsons, S. (1975) *J. Biol. Chem. 250*, 5669−5673.

Eads, J. C., Scapin, G., Xu, Y., Grubmeyer, C., & Sacchettini, J. C. (1994) *Cell 78*, 325−334.

Evans, S. V. (1993) *J. Mol. Graphics 11*, 134−138.

Goitein, R. K., Chelsky, D., & Parsons, S. (1978) *J. Biol. Chem. 253*, 2963−2971.

Green, P. C., Tripathi, R. L., & Kemp, R. G. (1993) *J. Biol Chem. 268*, 5085−5088.

Grubmeyer, C., Segura, E., & Dorfman, R. (1993) *J. Biol. Chem. 268*, 20299−20304.

Harmark, K., Anborgh, P. H., Merola, M., Clark, B. F. C., & Parmeggiani, A. (1992) *Biochemistry 31*, 7367−7372.

Hershey, H. V., & Taylor, M. (1986) *Gene 43*, 287−293.

Hove-Jensen, B., Harlow, K. W., King, C. J., & Switzer, R. L. (1986) *J. Biol. Chem. 261*, 6765−6771.

Hurley, J. H., Dean, A. M., Koshland, D. E., & Stroud, R. M. (1991) *Biochemistry 30*, 8671−8678.

Jones, T. A. (1985) *Methods Enzymol. 115*, 157−171.

Kabsch, W. (1988) *J. Appl. Crystallogr. 21*, 67−71.

Kraulis, P. J. (1991) *J. Appl. Crystallogr. 24*, 946−950.

Laskowsky, R. A., MacArthur, M. W., Moss, S. D., & Thornton, J. M. (1993) *J. Appl. Crystallogr. 26*, 283−291.

McClard, R. W., Black, M. J., Livingstone, L. R., & Jones, M. E. (1980) *Biochemistry 19*, 4699−4706.

Mentch, F., Parkin, D. W., & Schramm, V. L. (1987) *Biochemistry* 26, 921−930.

Murphy, J. E., Xu, X., & Kantrowitz, R. (1993) *J. Biol. Chem. 268*, 21497−21500.

Musik, W. D. L. (1981) *CRC Crit. Rev. Biochem. 11*, 1−34.

Nicholls, A., Sharp, K., & Honig, B. (1991) *Proteins: Struct., Funct. Genet. 11*, 281.

Ozturk, D. H., Dorfman, R. H., Scapin, G., Sacchettini, J. C., & Grubmeyer, C. (1995a) *Biochemistry 34*, 10755−10763.

Ozturk, D. H., Dorfman, R. H., Scapin, G., Sacchettini, J. C., & Grubmeyer, C. (1995b) *Biochemistry 34*, 10764−10770.

Rossmann, M. G., Liljas, A., Branden, C-I., & Banaszak, L. J. (1975) *Enzymes (3rd Ed.) 11A*, 61−102.

Scapin, G., Sacchettini, J. C., Dessen, A., Bhatia, M. B., & Grubmeyer, C. (1993) *J. Mol. Biol. 230*, 1304−1308.

Scapin, G., Grubmeyer, C., & Sacchettini, J. C. (1994) *Biochemistry 33*, 1287−1294.

Shostak, K., Christopherson, R. I., & Jones, M. E. (1990) *Anal. Biochem. 191*, 365−369.

Smith, J. L., Zaluzec, J., Wery, J. J.-P., Niu, L., Switzer, R. L., Zalkin, H., & Satow, Y. (1994) *Science 264*, 1427−1433.

Suttle, D. P., Bugg, B. Y., Winkler, J. K., & Kasalas, J. J. (1988) *Proc. Natl. Acad. Sci. U.S.A. 85*, 1754−1758.

Suttle, D. P., Becroft, D. M. O., & Webster, D. R. (1989) in *The Metabolic Basis of Inherited Disease* (Scriver, C. R., Beaudet, A. L., Sly, W. S., & Valle, D., Eds.) 6th ed., pp 1195−1226, McGraw-Hill, New York.

Tronrud, D. E., Ten Eyck, L. F., & Matthews, B. W. (1988) *Acta Crystallogr. A43*, 489−501.


BI950630R